Journal of Membrane Science 531 (2017) 122–128

Contents lists available at ScienceDirect

Journal of Membrane Science

journal homepage: www.elsevier.com/locate/memsci

Coaxially electrospun super-amphiphobic silica-based membrane for anti-surfactant-wetting membrane distillation

Yu-Xi Huang[a], Zhangxin Wang[a], Deyin Hou[b], Shihong Lin[a,*]

[a] Department of Civil and Environmental Engineering, Vanderbilt University, Nashville, TN 37235-1831, USA
[b] State Key Laboratory of Environmental Aquatic Chemistry, Research Center for Eco-Environmental Sciences, Chinese Academy of Sciences, Beijing 100085, China

ABSTRACT

Membrane distillation (MD) is a promising desalination technology that is capable of utilizing low-grade thermal energy to treat highly saline feed water. Conventional hydrophobic MD membranes limit the application of MD to desalination of relatively clean water without amphiphilic contaminants, as those amphiphilic constituents promote wetting of MD membrane and failure of the MD process. Here, we report a facile approach to fabricate superamphiphobic MD membranes with anti-surfactant-wetting property based on coaxial electrospinning. Silica nanoparticles were used as the sheath solution to create electrospun fibers with nanoscale roughness on individual fibers. After surface fluorination, the fabricated membrane exhibited superamphiphobicity as reflected by very high sessile drop contact angles with both water and oil. Robust MD performance in the presence of surfactants was observed with the superamphiphobic membrane, but not with commercial hydrophobic membranes or amphiphobic membrane without local nanoscale roughness.

1. Introduction

Membrane distillation (MD) is an emerging membrane-based thermal separation process for desalination [1]. Due to its distinct advantages of low capital cost, low operating pressure compared with reverse osmosis (RO), and low working temperature compared with conventional thermal distillation, MD has recently received growing interests in both academia and industry [2,3]. Because the driving force in an MD process is the cross-membrane water vapor pressure difference induced by temperature difference, which is relatively insensitive to feed water salinity, MD is a promising technological candidate for desalinating high salinity brine, such as shale gas produced water, which is challenging for RO to treat [4–6].

In an MD process, hydrophobic membranes made of polyvinylidene fluoride (PVDF), polypropylene (PP), or polytetrafluoroethylene (PTFE) are usually employed [5]. The membrane hydrophobicity is of critical importance, as it enables the membrane to serve as a barrier for direct liquid water permeation, which is imperative for salt rejection. However, amphiphilic organic contaminants and surfactants that commonly exist in saline wastewaters can readily adsorb onto a hydrophobic MD membrane, resulting in pore wetting and consequent failure of the MD process [7–9].

Recently, it has been shown that amphiphobic membrane, i.e., membrane that is resistant to wetting by both water and low surface tension liquids such as oil, can deliver robust MD performance even in the presence of surfactants [10–13]. Regardless of fabrication method, an amphiphobic membranes typically need to meet two requirements: first, the membrane surface should be made of low-surface-energy materials; second, the membrane should have reentrant pore structure, preferably at multiple scales [14–20]. Satiating these two requirements will facilitate the solution-membrane interfacial contact to be in the Cassie-Baxter state rather than the Wenzel state even if the solution surface tension is low, thereby preserving the indispensable air gap in the MD membrane pores [21–23].

Theoretically, a fibrous porous medium should have the reentrant geometry that is required for amphiphobicity [14]. In fact, several early studies in materials science fabricated amphiphobic surfaces using electrospinning technique to create fibrous networks with low-surface-energy materials [24,25]. In those cases, multiscale reentrant structure was not necessary to impart oleophobicity. However, those surfaces were not created as MD membranes and therefore were not tested for their anti-wetting performance in MD operations.

On the other hand, several recent studies on fabricating amphiphobic MD membranes modified commercial or pre-synthesized microporous membranes with silica nanoparticles (SiNPs) and TiO_2 nanoparticles using dip-coating to impart the multiscale reentrant

* Corresponding author.
E-mail address: shihong.lin@vanderbilt.edu (S. Lin).

http://dx.doi.org/10.1016/j.memsci.2017.02.044
Received 15 August 2016; Received in revised form 9 January 2017; Accepted 27 February 2017
Available online 28 February 2017

structure [10–12,26]. The modified membranes were then further fluorinated to attain low surface energy. The membranes fabricated using this approach not only exhibited resistance to wetting by both water and low-surface-tension liquids in air, but also showed promising anti-wetting property in MD tests with feed solution containing surfactants.

While this dip-coating approach for fabricating amphiphobic MD membranes has proven to be effective, it usually involves many steps of fabrication. Because SiNPs are typically negatively charged, the fibrous membranes were rendered positively charged to facilitate the attachment of SiNPs via electrostatic interaction. This was achieved by either modifying the silica fibrous networks using the positively charged amino-silane or by impregnating cationic surfactants into the polymer solution used for electrospinning [10–12]. Furthermore, while dip-coating is a simple laboratory-scale technique for surface modification, it is not an ideal technique for large-scale fabrication due to the relatively low utilization rate of the coating materials and the relatively long time to achieve a homogeneous and complete coating layer.

Electrospinning technique has been proven to be a universal and flexible method for fibrous membrane fabrication [27–29]. Compatible with many different types of polymer precursors, electrospinning is capable of preparing membranes with high porosity as well as tailorable thickness, pore size, and surface wettability [24,30–35]. Moreover, fibers with core-sheath structure can also be obtained using coaxial electrospinning, which enables efficient formation of fibers with different chemical compositions and functional properties along the radial direction. Various applications based on coaxial electrospun fibrous materials have been reported for energy storage, drug delivery and tissue engineering [36–39]. It is possible to employ coaxial electrospinning with nanoparticles suspension as the sheath solution to create fibrous membranes with local reentrant structure on individual fibers. If proven viable, this coaxial spinning technique can be a very convenient approach to fabricate amphiphobic membranes with highly efficient utilization of the nanoparticles.

There are two primary objectives for this study. First, we want to demonstrate that we can use co-axial electrospinning to create a fibrous network with multiscale reentrant structure, and that such a fibrous network is amphiphobic and can function as an MD membrane with robust resistance to surfactant wetting. Secondly, we also want to compare electrospun fibrous networks, with and without the additional level of reentrant structure imparted by the presence of nanoparticles, in terms of their anti-wetting performance in MD processes.

In this study, we develop a facile method based on electrospinning for the fabrication of inorganic silica-based MD membranes with in-air amphiphobicity. We first prepared two different silica-based membranes, one with single-scale reentrant structure created by mono-axial electrospinning, and the other with multi-scale reentrant structure enabled by coaxial electrospinning. The electrospun silica-based membranes were modified by fluoroalkylsilane to acquire low surface energy. We then conducted a series of materials characterizations regarding the morphological, chemical, and surface wetting properties of the fabricated membranes. Finally, we evaluated the anti-wetting performance of the fabricated membranes in direct contact membrane distillation (DCMD) experiments with a model surfactant, sodium dodecylsulfate (SDS), in the feed solution to promote wetting.

2. Materials and methods

2.1. Chemicals

Polyvinyl alcohol (PVA, 99%, MW=89,000–98,000), tetraethyl orthosilicate (TEOS, 98%), silica NPs (Ludox HS-40), 1H,1H,2H,2H-perfluorodecyltriethoxysilane (FAS, 97%), sodium dodecyl sulfate (SDS, 99%), and mineral oil were purchased from Sigma-Aldrich and used without purification. Ortho-phosphoric acid (85%) was procured from Fisher Scientific. Deionized water (DI water) was used throughout the experiment. PVDF membranes with a nominal pore size of 0.45 μm were purchased from GE Healthcare Life Sciences.

2.2. Precursor solutions for electrospinning

The solution for the mono-axial electrospinning was a mixture of PVA and silica gel formed by hydrolysis of TEOS [24]. Briefly, a 10 wt% PVA stock solution was prepared by dissolving PVA in DI water at 80 °C. A silica gel suspension was prepared by dropwise addition of H_3PO_4 to a solution of TEOS under vigorous stirring at room temperature for 6 h, with the molar composition of TEOS:H_3PO_4:H_2O being 1:0.01:11. The formed silica gel was then mixed with the PVA stock solution with a mass ratio of 1:1 for another 6 h.

In coaxial electrospinning, the as-prepared PVA/silica solution was used as the core solution. To prepare the sheath solution, 5 g of Ludox SiNPs suspension (40% w/w), was dispersed in 15 g of the aqueous PVA stock solution. The mixture was stirred for 1 h to ensure the homogeneous dispersion of SiNPs. In both cases, the PVA in the core solution served as a viscosity enhancer and as a polymeric binder to facilitate fiber formation. In the case of coaxial electrospinning, the PVA in the sheath solution also served to immobilize the SiNPs. The PVA was removed in later stage of the fabrication by calcination.

2.3. Electrospinning parameters

The electrospinning was conducted using a commercial electrospinning instrument with a rotating drum collector (TL-01, Tongli Tech., China). For mono-axial electrospinning, the feeding rate of the PVA/silica solution was controlled to be 0.6 mL h^{-1} using a syringe pump. The spun fibers were collected on an aluminum foil covering a grounded stainless cylindrical drum with a rotating speed of 150 rpm. The applied voltage was 15 kV, and the distance between the spinneret and the rotating drum collector was 20 cm.

In coaxial electrospinning, the total feeding rate was also 0.6 mL h^{-1}, with both the core and the sheath solutions contributing 0.3 mL h^{-1}. Other parameters were the same as that in the monoaxial electrospinning, except that a higher voltage (23 kV) was employed. In both cases, the temperature was 26 °C and the spinning time was 30 h. In the following discussion, the PVA blended electrospun silica fibrous membranes (SFM) with and without the addition of SiNPs are referred to as PVA@SFM and PVA@SiNPs-SFM, respectively.

2.4. Membrane calcination and fluorination

The as-prepared PVA@SFM and PVA@SiNPs-SFM were calcined at 800 °C in air for 2 h to remove the PVA binder. In the case of coaxially spun membrane, the calcination also served to sinter the SiNPs onto the underlying silica fibers to ensure robust attachment. The inorganic membranes after calcination were highly hydrophilic due to the strong interaction between silica and water. To reduce the surface energy of the membrane, surface fluorination was carried out by immersing the membrane into a hexane solution of 3 wt% FAS for 24 h at room temperature. The membranes were then dried in air at 80 °C in an oven. The FAS modified SFM and SiNPs-SFM are denoted as FAS@SFM and FAS@SiNPs-SFM, respectively. The schematics of the membrane preparation are shown in Fig. 1.

2.5. Membrane characterization

The morphology of fabricated membranes was characterized by scanning electron microscopy (SEM, Zeiss Merlin) and transmission electron microscopy (TEM, FEI Tecnai Osiris). To prepare the TEM sample, the as-prepared membranes were cut into small pieces and then ultra-sonicated in ethanol for 10 min. The supernatant containing the dislodged fibers was used as TEM samples. Fourier transform

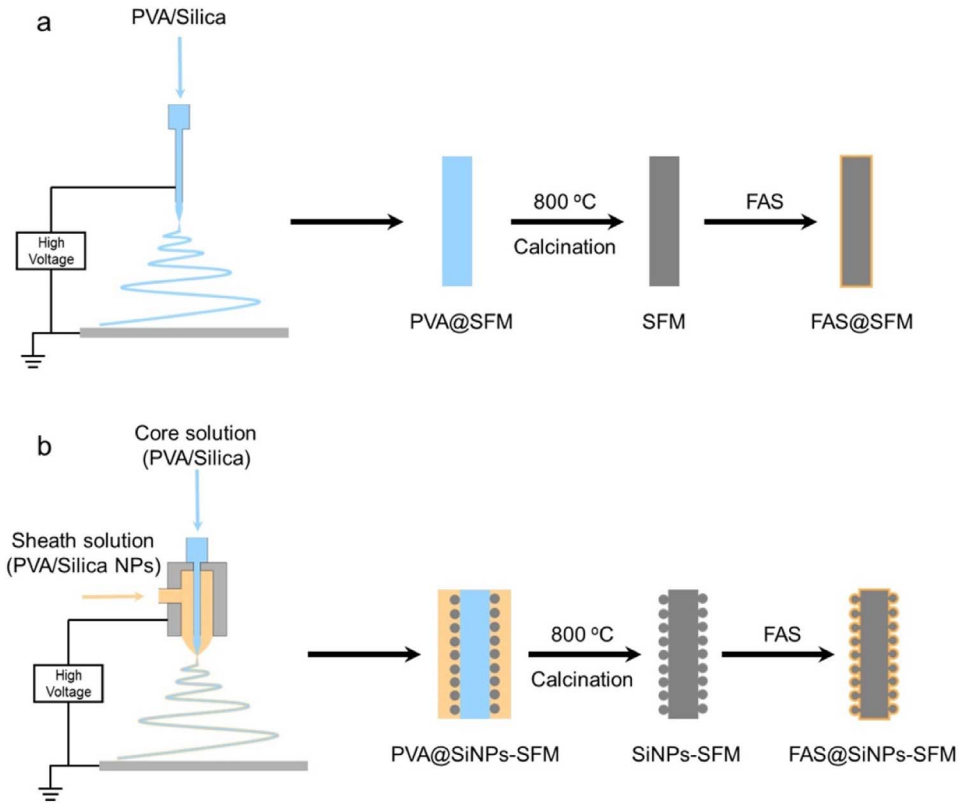

Fig. 1. Schematics of the preparation procedures for (a) FAS@SFM and (b) FAS@SiNPs-SFM. The fabrication of the FAS@SFM involved the creation of a fibrous network via monoaxial electrospinning using a blend of PVA/silica as the precursor. The electrospun fibrous membrane was then calcined to obtain the SFM which is fluorinated by FAS to result in FAS@SFM. The fabrication procedures of the FAS@SiNPs-SFM were similar to that of the FAS@SFM with the exception that coaxial, instead of monoaxial, electrospinning was used with a suspension of SiNPs as the sheath solution. The SiNPs in the sheath solution created local roughness on the fiber surface.

infrared (FTIR) spectroscopy was performed using an FTIR spectrometer (Bruker Tensor 27). The pore size distribution of the membrane was measured using capillary flow porometer (Poroflux 1000, IB-GT GmbH, Germany). Sessile drop contact angles (CA) were measured with an optical tensiometer (Theta Lite, Biolin Scientific) using both water and mineral oil as the liquid phases. Lastly, we also measured the liquid entry pressure (LEP) of the membrane samples using water as well as SDS solutions of the concentrations tested in the MD experiments. The LEP was measured by gradually increasing the applied hydraulic pressure in an Amicon® cell mounted with the membrane sample until non-zero flux was observed.

2.6. Membrane distillation experiments

The fabricated membrane samples with an effective area of 20 cm^2 were tested in a custom made MD cell. Direct contact MD (DCMD) with concurrent flow was the adopted system configuration in these experiments. The feed stream was a 35 g L^{-1} NaCl solution at a temperature of 60 °C, whereas the distillate stream was DI water at a temperature of 20 °C. The mass and conductivity of the distillate were recorded constantly, from which the real time flux and salt rejection were calculated. We intentionally maintained the flowrates for the feed and distillate streams to be 0.4 L min^{-1} and 0.2 L min^{-1}, respectively, which resulted in a higher hydraulic pressure in the feed stream (9 kPa) than in the distillate stream (3 kPa) in this specific experimental setup. In this way, if any pore wetting occurs, the increase in distillate salinity as a consequence of the compromised salt rejection rate will become the unambiguous evidence. During the course of the MD experiments, SDS was added sequentially to the feed solution in a way such that the SDS concentrations of the feed solution after each addition were 0.1, 0.2, 0.3, and 0.4 mM. The SDS was added to the feed stream to reduce the surface tension of the solution and thereby to induce pore wetting, if the membranes were wettable.

3. Results and discussion

3.1. Morphology and surface chemistry

The SEM images of the fabricated membranes with and without coaxial spinning are shown in Fig. 2. Compared to the smooth fibers in the SFM (Fig. 2a), spindle structures were observed in the SiNPs-SFM (Fig. 2d), which could be attributed to the lower viscosity of the sheath solution than the core solution [40]. For this reason, the SiNPs-SFM showed larger mean fiber diameter and standard deviation (324.8 ± 124.4 nm) compared with the SFM (188.9 ± 16.4 nm). TEM image of the SFM (Fig. 2c) showed no distinct crystalline structure, indicating that the silica fiber in SFM was amorphous (Fig. 2c). For the coaxial electrospun SiNPs-SFM, a homogeneous and complete coating of the fibers by SiNPs was clearly observed (Fig. 2e and f), suggesting that the core-sheath structure was successfully achieved. The presence of silica NPs introduced local roughness and reentrant structure on the fiber surface, which could potentially improve the robustness of wetting resistance. The effective pore size for the SFM and SiNPs-SFM were 0.85 ± 0.12 and 0.84 ± 0.15 μm, respectively, as suggested by results from capillary flow porometry.

The changes of surface chemistry during the membrane fabrication were characterized by FTIR, and the results are shown in Fig. 3. For the PVA@SFM and PVA@SiNPs-SFM prior to calcination, the broad band located at about 3300 cm^{-1} is the typical vibration originating from O-H stretching. The weak but identifiable peak at 2940 cm^{-1} indicated the presence of C-H bond. The peaks located at around 1650 cm^{-1} and 1420 cm^{-1} could be attributed to the C=O and C-C stretching, respectively [41]. These characteristic absorption peaks verified the presence of PVA. Besides, the strong absorption band from 1150 to 1050 cm^{-1}

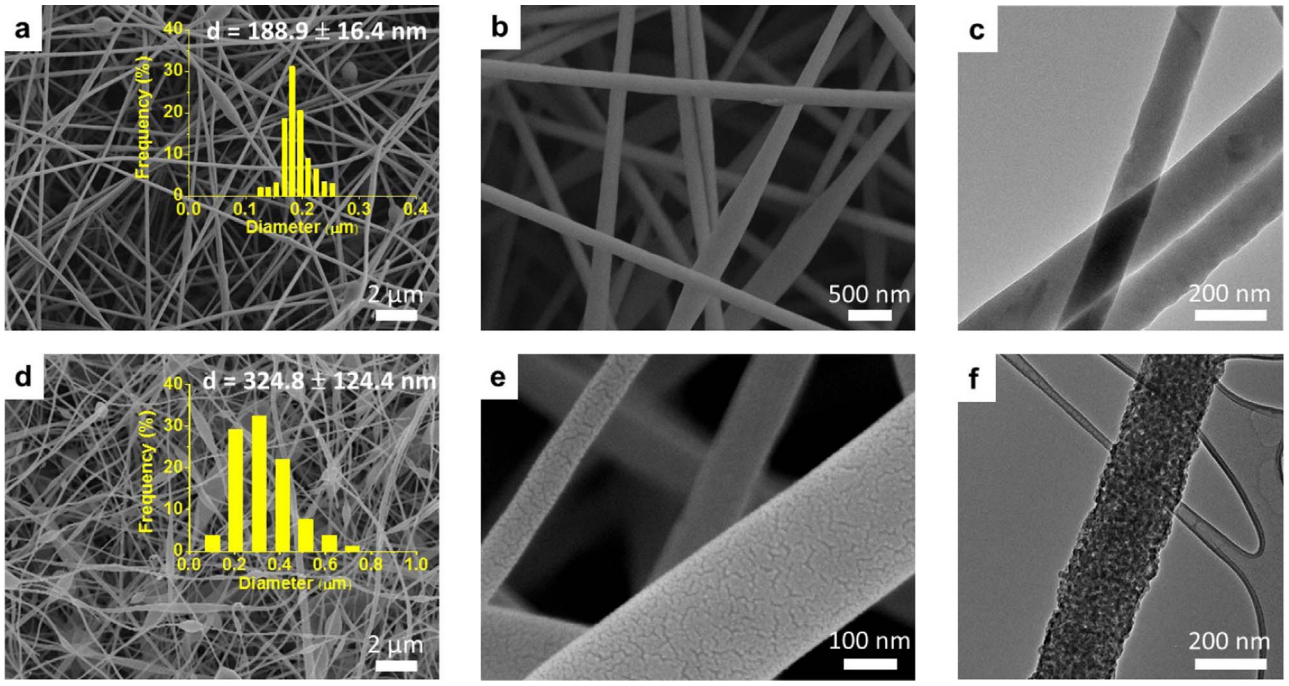

Fig. 2. SEM and TEM images of the SFM (a, b for SEM and c for TEM) and coaxially electrospun SiNPs-SFM (d, e for SEM and f for TEM). The insets in (a) and (d) show the diameter distributions of the nano fibers. The mean diameters for SFM and SiNPs-SFM are 188.9 ± 16.4 and 324.8 ± 124.4 nm, respectively. The SEM and TEM images in (e and d) clearly show the presence of SiNPs on the fiber surface.

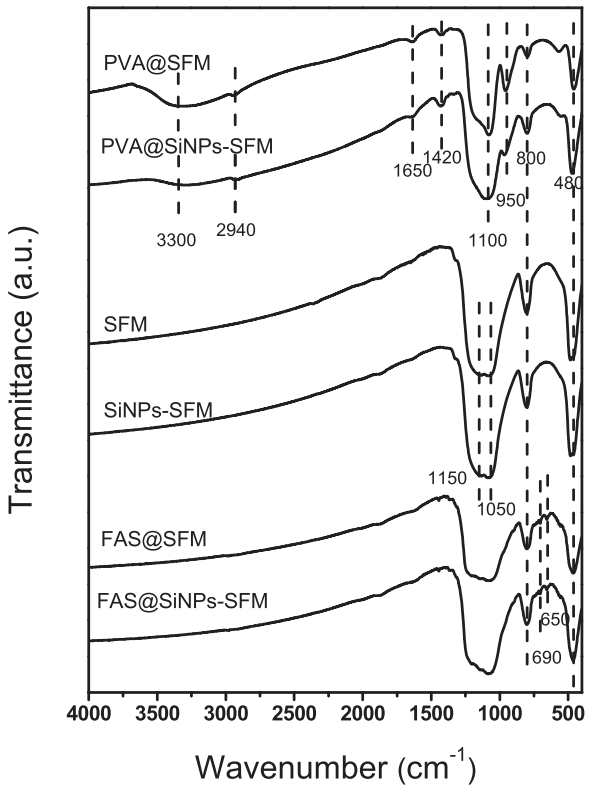

Fig. 3. FTIR spectra of the membranes in different preparation stages. Arrows indicate the approximated absorption band/peak location. Vibrational modes are shown for O–H (~3300 cm^{-1}), C–H (~2940 cm^{-1}), C=O (~1650 cm^{-1} and ~1150–1050 cm^{-1}), C–C (1420 cm^{-1}), Si–O (~1150–1050 cm^{-1}), Si–OH (950 cm^{-1}), Si–O–Si (~800 cm^{-1} and ~480 cm^{-1}), and C–F (~1100 cm^{-1} to 1200 cm^{-1}, 690 cm^{-1}, and 650 cm^{-1}).

was the combination of C–O and Si–O vibrations [42]. The symmetric stretching vibrations of Si–O–Si appeared at 800 cm^{-1}, while its bending mode appeared at 480 cm^{-1}. Since the silica was prepared through TEOS hydrolysis, Si–OH bond was also observable at around 950 cm^{-1} [43].

After calcination at 800 °C for 2 h, PVA was completely removed, as evidenced by the disappearance of the absorption peaks characteristic of PVA. Meanwhile, the Si–OH absorption peak also disappeared, the main absorption peaks remaining in the spectra were those characteristic of Si–O. Such results confirmed that the SFM and SiNPs-SFM after calcination were inorganic membranes composed of SiO_2. FTIR spectra of the FAS modified membranes were similar to that of the calcined SFM and SiNPs-SFM before fluorination. According to previous studies, the absorption bands for C–F bond locate from about 1100 cm^{-1} to 1200 cm^{-1} and thus overlap with that of the Si–O [44]. Nevertheless, the shape change of the absorption band from around 1000 cm^{-1} to 1300 cm^{-1}, which is believed to result from the presence of C–F bonds, could still be clearly identified. In addition, small peaks at 690 cm^{-1} and 650 cm^{-1} could also be attributed to the C-F bond. Overall, these results showed that the membrane surface had been successfully modified with FAS.

3.2. Wetting properties

The SFM and SiNPs-SFM after calcination were both superhydrophilic, as indicated by the instant wicking by water. After surface fluorination with the low-surface-energy FAS, both membranes exhibited amphiphobicity. The water and oil CAs for the FAS@SFM were 134.4 ± 2.8° and 117.3 ± 7.2°, respectively (Table 1). In contrast, a commercial hydrophobic PVDF membrane had a water CA of 107.2 ±

Table 1
Sessile drop CA and LEP for the three membrane samples.

	DI water (°)	Mineral oil (°)	LEP[a] (kPa)
FAS@SFM	134.4 ± 2.8	117.3 ± 7.2	44.7 ± 4.1
FAS@SiNPs-SFM	154.2 ± 3.6	149.0 ± 11.7	91.3 ± 6.6
commercial PVDF	107.2 ± 4.7	0 (wicking)	119.0 ± 8.0

[a] The LEPs were measured with water, although LEPs measured with SDS solutions yielded essentially the same results.

4.6° and was wicked by mineral oil. The fact that FAS@SFM without SiNPs was also resistant to oil wetting suggests that electrospun fibrous structure itself already had the reentrant structure required for achieving oleophobicity. As we mentioned, electrospinning technique has been employed in previous studies to create amphiphobic surfaces [24,25].

In comparison, the FAS@SiNPs-SFM were superamphiphobic, with its water and oil CAs measured to be 154.2 ± 3.6° and 149 ± 11.7°, respectively. The higher CA could be attributed to the core-sheath structure of the FAS@SiNPs-SFM with which the SiNPs on the individual fibers provided an additional level of roughness and reentrant texture. The importance of hierarchical texture in imparting superamphiphobicity has been theoretically addressed in literature [20]. In our case, it can be mathematically proved that the second level roughness on the fiber enhances the CA of the fibrous membrane and renders the FAS@SiNPs-SFM superamphiphobic (Appendix A).

The LEP measurements suggest that the presence of a second level roughness also enhanced the LEP of the membrane. The LEPs of both the electrospun membranes were lower than that of the PVDF membrane, most likely due to the smaller effective pore size of the PVDF membrane (0.45 μm nominal size). Surprisingly, the addition of SDS (up to 5 mM) did not seem to affect the LEP even though the overall surface tension of the solution was reduced by SDS: the LEPs measured with both water and SDS solutions were essentially the same for all three membranes. Similar surprising phenomenon was also observed regarding the water CA of the membranes, which was consistent with previous finding that the CA on a PVDF membrane measured using DI water was very close to that measured using a SDS solution with a concentration up to half of its critical micelle concentration (CMC) [10]. Although no major difference was observed in the membrane wetting when the LEP and CA were measured using solution containing different SDS concentration, wetting of MD by feed solution of very low SDS concentration was detected as described in the following section as well as in literature [10–12].

3.3. Membrane distillation performance in the presence of surfactants

The FAS@SFM, FAS@SiNPs-SFM, and the commercial PVDF membrane (as reference) were tested in DCMD during which SDS was added progressively to promote membrane wetting. The initial water fluxes for FAS@SFM, FAS@SiNPs-SFM, and PVDF membranes were 17.1 ± 0.9 L m^{-2} h^{-1}, 21.9 ± 1.2 L m^{-2} h^{-1}, and 45.9 ± 1.9 L m^{-2} h^{-1} respectively. The salt rejection rates were 100% in all case without the addition of SDS (Fig. 4).

With the addition of SDS into the feed stream, however, severe wetting was observed on the FAS@SFM and PVDF membrane as indicated by the dramatic changes of water flux and salt rejection rate. Because we intentionally controlled the feed hydraulic pressure to be higher than that of the distillate, water in the wetted pores unequivocally flowed from the feed stream to the distillate stream and thereby increased both the transmembrane water flux (including liquid and vapor) and the solute flux. Interestingly, the FAS@SFM seems to be even more susceptible to SDS wetting than the hydrophobic but oleophilic PVDF membrane, as the changes of water flux and salt rejection was more severe for the FAS@SFM than for PVDF membrane when the SDS concentration of the feed stream was raised to 0.2 mM and above. This is probably due to the higher effective pore size of FAS@SFM membrane (~0.85 μm) compared to that of the commercial PVDF membrane (~0.45 μm). Once wetted, the rejection rates for both membranes became unacceptable for any practical MD application.

In comparison, the performance of FAS@SiNPs-SFM remained stable over the course of the entire MD test. Neither water flux nor the salt rejection rate was affected by the SDS dosing even up to a concentration of 0.4 mM, suggesting the robust performance of the co-axially spun FAS@SiNPs-SFM against surfactant wetting. Our

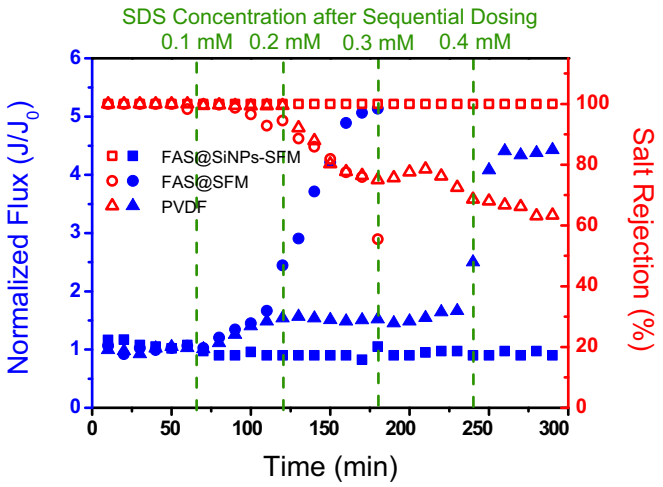

Fig. 4. Water flux (blue) and salt rejection rate (red) for the fabricated FAS@SiNPs-SFM (square), FAS@SFM (circle), and the commercial PVDF membrane (triangle). The green dash lines indicate the addition of SDS, with the numbers on the top representing the final SDS concentration of the feed solution after the addition. The MD experiment for the FAS@SFM was stopped prematurely because the salt rejection rate dropped to an unacceptable level. The water fluxes are normalized to the initial flux of each membrane. The initial water fluxes for FAS@SiNPs-SFM, FAS@SFM, and PVDF membranes were 21.9 ± 1.2 L m^{-2} h^{-1}, 17.1 ± 0.9 L m^{-2} h^{-1}, and 45.9 ± 1.9 L m^{-2} h^{-1}, respectively. (For interpretation of the references to color in this figure legend, the reader is referred to the web version of this article.)

results suggest that surfactant induced membrane wetting in MD could not be simply explained by the fact that the added surfactants reduced the surface tension of the feed solution and thereby lowered the LEP. First of all, as we mentioned in Section 3.2, the presence of the SDS did not seem to reduce the LEP of the membranes. Secondly, if the LEP were the determining factor for wetting, the FAS@SiNPs-SFM should be more susceptible to wetting than PVDF as the measured LEP for FAS@SiNPs-SFM was lower than that of LEP, which was inconsistent with our experimental observation. Last but not least, the hydraulic pressure in the feed channel was measured to be only 9 kPa (vs 3 kPa for the distillate channel), which was only a very small fraction of the LEP of any membrane tested. These observations together seem to rule out the possible explanation of membrane wetting that the SDS reduced the surface tension of the feed solution and thus the LEP below the feed hydraulic pressure. We speculate that membrane wetting in MD was possibly induced by the adsorption of surfactants onto the membrane surface which rendered the membrane hydrophilic over time. Further investigation of MD membrane wetting by surfactant is required to elucidate its detailed mechanism.

The stronger anti-wetting property of FAS@SiNPs-SFM as compared to FAS@SFM is attributable to the second scale of roughness introduced by the SiNPs on the fiber surface, which rendered the local wetting of individual fibers more difficult. The importance of multiscale reentrant structure on enhancing the superhydrophobicity or amphiphobicity of membranes have been relatively well understood [14,15,18,20]. In previous studies, the additional local reentrant structure was imparted by coating fluorinated TiO_2 or SiO_2 nanoparticles onto the existing membrane substrates, which has been shown to be very effective in mitigating membrane wetting [10–12,26]. Here, we demonstrate for the first time that an effective anti-wetting MD membrane with hierarchical roughness can also be fabricated by leveraging on coaxial electrospinning to create a second scale of reentrant structure.

4. Conclusions

In this study, we fabricated a silica-based fibrous membrane with core-sheath structure using coaxial electrospinning technique. The

resulting membrane, FAS@SiNPs-SFM, has two scales of reentrant textures, with the first scale provided by the fibrous network and the second scale enabled by the SiNPs on the surface of individual fibers. The FAS@SiNPs-SFM has been shown to be superamphiphobic, as compared to amphiphobic FAS@SFM without SiNPs, and the hydrophobic but oleophilic commercial PVDF membrane. The results from MD experiments using feed solution with a common surfactant, SDS, suggest that only FAS@SiNPs-SFM could sustain robust MD operation in the presence of relatively high concentration of surfactants, whereas the FAS@SFM and the PVDF membrane both failed due to membrane wetting. The superamphiphobicity as well as the superior anti-wetting performance of the FAS@SiNPs-SFM could both be attributed to the additional scale of reentrant structure enabled by the SiNPs on the surface of individual fibers. The coaxial electrospinning technique reported herein is an alternative approach to the conventional nanoparticle dip-coating approach to create such multiscale structure. More importantly, it also opens a new path to facile fabrication of superamphiphobic membranes with the ability to precisely control SiNPs loading, which is important for scaling up the fabrication of superamphiphobic MD membranes.

Acknowledgements

The authors acknowledge the financial support from Bureau of Reclamation, Department of Interior, via DWPR Agreement R15AC00088.

Appendix A. Analysis of the effect of dual-scale reentrant texture on contact angle

Quantitatively, the apparent CA for surface with dual-scale reentrant texture, θ_2^*, can be described using the following equation derived by applying the Cassie-Baxter relation twice [45,46]:

$$cos\theta_2^* = (1-f_{LG,m})\left[\left(1-f_{LG,f}\right)cos\theta - f_{LG,f}\right] - f_{LG,m}$$

where θ is the intrinsic CA of the material, which could only be measured with a perfectly non-textured surface made of the same material (FAS in this case), $f_{LG,f}$ is the areal fraction of the liquid-gas interface at the single fiber scale which corresponds to the contact of liquid with air trapped between SiNPs on a fiber, and $f_{LG,m}$ is the areal fraction of the liquid-gas interface at the membrane scale which concerns the contact of liquid with air trapped between fibers. For FAS@SFM, only one level of reentrant texture is present, and the above equation is thus reduced to:

$$cos\theta_1^* = (1-f_{LG,m})cos\theta - f_{LG,m}$$

where θ_1^* is the apparent CA for a fibrous network where the only reentrant texture is created by the fibers themselves. It can be easily proved that θ_1^* is always lower than θ_2^* because the sufficient condition for $\theta_1^* < \theta_2^*$ is $cos\theta_2^* < cos\theta_1^*$ when the θ is from 0° to 180°, which is indeed the case as shown by the following equation obtained from Eqs. 1 and 2:

$$cos\theta_2^* - cos\theta_1^* = -(1-f_{LG,m})f_{LG,f}(1+cos\theta) < 0$$

This analysis suggests that the second scale reentrant structure was responsible for enhancing the amphiphobicity of the membrane and render it superamphiphobic.

References

[1] K.W. Lawson, D.R. Lloyd, Membrane distillation, J. Membr. Sci. 124 (1997) 1–25.
[2] S. Al-Obaidani, E. Curcio, F. Macedonio, G. Di Profio, H. Al-Hinai, E. Drioli, Potential of membrane distillation in seawater desalination: thermal efficiency, sensitivity study and cost estimation, J. Membr. Sci. 323 (2008) 85–98.
[3] A. Alkhudhiri, N. Darwish, N. Hilal, Membrane distillation: a comprehensive review, Desalination 287 (2012) 2–18.
[4] S. Lin, N.Y. Yip, M. Elimelech, Direct contact membrane distillation with heat recovery: thermodynamic insights from module scale modeling, J. Membr. Sci. 453 (2014) 498–515.
[5] P. Wang, T.-S. Chung, Recent advances in membrane distillation processes: membrane development, configuration design and application exploring, J. Membr. Sci. 474 (2015) 39–56.
[6] D.L. Shaffer, L.H. Arias Chavez, M. Ben-Sasson, S. Romero-Vargas Castrillon, N.Y. Yip, M. Elimelech, Desalination and reuse of high-salinity shale gas produced water: drivers, technologies, and future directions, Environ. Sci. Technol. 47 (2013) 9569–9583.
[7] A.C.M. Franken, J.A.M. Nolten, M.H.V. Mulder, D. Bargeman, C.A. Smolders, Wetting criteria for the applicability of membrane distillation, J. Membr. Sci. 33 (1987) 315–328.
[8] S. Goh, J. Zhang, Y. Liu, A.G. Fane, Fouling and wetting in membrane distillation (MD) and MD-bioreactor (MDBR) for wastewater reclamation, Desalination 323 (2013) 39–47.
[9] P.-J. Lin, M.-C. Yang, Y.-L. Li, J.-H. Chen, Prevention of surfactant wetting with agarose hydrogel layer for direct contact membrane distillation used in dyeing wastewater treatment, J. Membr. Sci. 475 (2015) 511–520.
[10] J. Lee, C. Boo, W.-H. Ryu, A.D. Taylor, M. Elimelech, Development of omniphobic desalination membranes using a charged electrospun nanofiber scaffold, ACS Appl. Mater. Interfaces 8 (2016) 11154–11161.
[11] S. Lin, S. Nejati, C. Boo, Y. Hu, C.O. Osuji, M. Elimelech, Omniphobic membrane for robust membrane distillation, Environ. Sci. Technol. Lett. 1 (2014) 443–447.
[12] C. Boo, J. Lee, M. Elimelech, Engineering surface energy and nanostructure of microporous films for expanded membrane distillation applications, Environ. Sci. Technol. 50 (2016) 8112–8119.
[13] C. Boo, J. Lee, M. Elimelech, Omniphobic polyvinylidene fluoride (PVDF) membrane for desalination of shale gas produced water by membrane distillation, Environ. Sci. Technol. 50 (2016) 12275–12282.
[14] A. Tuteja, W. Choi, M. Ma, J.M. Mabry, S.A. Mazzella, G.C. Rutledge, G.H. McKinley, R.E. Cohen, Designing superoleophobic surfaces, Science 318 (2007) 1618–1622.
[15] A. Tuteja, W. Choi, J.M. Mabry, G.H. McKinley, R.E. Cohen, Robust omniphobic surfaces, Proc. Natl. Acad. Sci. USA 105 (2008) 18200–18205.
[16] B. Wang, W. Liang, Z. Guo, W. Liu, Biomimetic super-lyophobic and super-lyophilic materials applied for oil/water separation: a new strategy beyond nature, Chem. Soc. Rev. 44 (2015) 336–361.
[17] S. Pan, A.K. Kota, J.M. Mabry, A. Tuteja, Superomniphobic surfaces for effective chemical shielding, J. Am. Chem. Soc. 135 (2013) 578–581.
[18] T.L. Liu, C.-J.C. Kim, Turning a surface superrepellent even to completely wetting liquids, Science 346 (2014) 1096–1100.
[19] A.K. Kota, W. Choi, A. Tuteja, Superomniphobic surfaces: design and durability, MRS Bull. 38 (2013) 383–390.
[20] A.K. Kota, G. Kwon, A. Tuteja, The design and applications of superomniphobic surfaces, NPG Asia Mater. 6 (2014) e109.
[21] L. Zhang, Y. Zhong, D. Cha, P. Wang, A self-cleaning underwater superoleophobic mesh for oil-water separation, Sci. Rep. 3 (2013) 2326.
[22] Y. Liao, R. Wang, A.G. Fane, Engineering superhydrophobic surface on poly(-vinylidene fluoride) nanofiber membranes for direct contact membrane distillation, J. Membr. Sci. 440 (2013) 77–87.
[23] Y. Liao, R. Wang, A.G. Fane, Fabrication of bioinspired composite nanofiber membranes with robust superhydrophobicity for direct contact membrane distillation, Environ. Sci. Technol. 48 (2014) 6335–6341.
[24] M. Guo, B. Ding, X. Li, X. Wang, J. Yu, M. Wang, Amphiphobic nanofibrous silica mats with flexible and high-heat-resistant properties, J. Phys. Chem. C 114 (2010) 916–921.
[25] J. Lin, F. Tian, B. Ding, J. Yu, J. Wang, A. Raza, Facile synthesis of robust amphiphobic nanofibrous membranes, Appl. Surf. Sci. 276 (2013) 750–755.
[26] A. Razmjou, E. Arifin, G. Dong, J. Mansouri, V. Chen, Superhydrophobic modification of TiO_2 nanocomposite PVDF membranes for applications in mem-

brane distillation, J. Membr. Sci. 415–416 (2012) 850–863.
[27] F.E. Ahmed, B.S. Lalia, R. Hashaikeh, A review on electrospinning for membrane fabrication: challenges and applications, Desalination 356 (2015) 15–30.
[28] M. Inagaki, Y. Yang, F. Kang, Carbon nanofibers prepared via electrospinning, Adv. Mater. 24 (2012) 2547–2566.
[29] P.S. Kumar, J. Sundaramurthy, S. Sundarrajan, V.J. Babu, G. Singh, S.I. Allakhverdiev, S. Ramakrishna, Hierarchical electrospun nanofibers for energy harvesting, production and environmental remediation, Energy Environ. Sci. 7 (2014) 3192–3222.
[30] E.S. Cozza, O. Monticelli, E. Marsano, P. Cebe, On the electrospinning of PVDF: influence of the experimental conditions on the nanofiber properties, Polym. Int. 62 (2013) 41–48.
[31] Z.-Q. Dong, X.-H. Ma, Z.-L. Xu, Z.-Y. Gu, Superhydrophobic modification of PVDF–SiO_2 electrospun nanofiber membranes for vacuum membrane distillation, RSC Adv. 5 (2015) 67962–67970.
[32] L. Huang, J.T. Arena, S.S. Manickam, X. Jiang, B.G. Willis, J.R. McCutcheon, Improved mechanical properties and hydrophilicity of electrospun nanofiber membranes for filtration applications by dopamine modification, J. Membr. Sci. 460 (2014) 241–249.
[33] F. Kayaci, Z. Aytac, T. Uyar, Surface modification of electrospun polyester nanofibers with cyclodextrin polymer for the removal of phenanthrene from aqueous solution, J. Hazard. Mater. 261 (2013) 286–294.
[34] Y. Liao, C.-H. Loh, R. Wang, A.G. Fane, Electrospun superhydrophobic membranes with unique structures for membrane distillation, ACS Appl. Mater. Interfaces 6 (2014) 16035–16048.
[35] Y. Liao, R. Wang, M. Tian, C. Qiu, A.G. Fane, Fabrication of polyvinylidene fluoride (PVDF) nanofiber membranes by electro-spinning for direct contact membrane distillation, J. Membr. Sci. 425–426 (2013) 30–39.
[36] H. Qu, S. Wei, Z. Guo, Coaxial electrospun nanostructures and their applications, J. Mater. Chem. A 1 (2013) 11513.
[37] D. Han, A.J. Steckl, Superhydrophobic and oleophobic fibers by coaxial electrospinning, Langmuir 25 (2009) 9454–9462.
[38] T. Song, Y. Zhang, T. Zhou, C.T. Lim, S. Ramakrishna, B. Liu, Encapsulation of self-assembled FePt magnetic nanoparticles in PCL nanofibers by coaxial electrospinning, Chem. Phys. Lett. 415 (2005) 317–322.
[39] D.-G. Yu, J. Zhou, N.P. Chatterton, Y. Li, J. Huang, X. Wang, Polyacrylonitrile nanofibers coated with silver nanoparticles using a modified coaxial electrospinning process, Int. J. Nanomed. 7 (2012) 5725–5732.
[40] H. Fong, I. Chun, D.H. Reneker, Beaded nanofibers formed during electrospinning, Polymer 40 (1999) 4585–4592.
[41] H.S. Mansur, R.L. Oréfice, A.A.P. Mansur, Characterization of poly(vinyl alcohol)/poly(ethylene glycol) hydrogels and PVA-derived hybrids by small-angle X-ray scattering and FTIR spectroscopy, Polymer 45 (2004) 7193–7202.
[42] V. Georgakilas, A.B. Bourlinos, R. Zboril, C. Trapalis, Synthesis, characterization and aspects of superhydrophobic functionalized carbon nanotubes, Chem. Mater. 20 (2008) 2884–2886.
[43] R. Al-Oweini, H. El-Rassy, Synthesis and characterization by FTIR spectroscopy of silica aerogels prepared using several Si(OR)4 and R′′Si(OR′)3 precursors, J. Mol. Struct. 919 (2009) 140–145.
[44] G. Legeay, A. Coudreuse, J.-M. Legeais, L. Werner, A. Bulou, J.-Y. Buzaré, J. Emery, G. Silly, AF fluoropolymer for optical use: spectroscopic and surface energystudies; comparison with other fluoropolymers, Eur. Polym. J. 34 (1998) 1457–1465.
[45] E. Bittoun, A. Marmur, The role of multiscale roughness in the lotus effect: is it essential for super-hydrophobicity?, Langmuir 28 (2012) 13933–13942.
[46] S.S. Chhatre, W. Choi, A. Tuteja, K.-C. Park, J.M. Mabry, G.H. McKinley, R.E. Cohen, Scale dependence of omniphobic mesh surfaces, Langmuir 26 (2010) 4027–4035.